Available online at www.sciencedirect.com

ScienceDirect

International Journal of Solids and Structures 44 (2007) 5247–5271

INTERNATIONAL JOURNAL OF SOLIDS and STRUCTURES

www.elsevier.com/locate/ijsolstr

# Interfacial stress analysis of a thin plate bonded to a rigid substrate and subjected to inclined loading

H. Yuan [a,b], J.F. Chen [c,*], J.G. Teng [a], X.Z. Lu [d]

[a] *Department of Civil and Structural Engineering, The Hong Kong Polytechnic University, Hong Kong, China*
[b] *Department of Mechanics and Civil Engineering, Jinan University, Guangzhou 510632, China*
[c] *Institute for Infrastructure and Environment, Edinburgh University, Edinburgh EH9 3JN, Scotland, UK*
[d] *Department of Civil Engineering, Tsinghua University, Beijing, China*

Received 12 December 2005; received in revised form 3 November 2006
Available online 28 December 2006

**Abstract**

The so-called peel test, in which a thin plate bonded to a substrate is subjected to an inclined pulling force, has been widely used to characterise the bond behaviour of adhesives. This paper presents an analytical solution for the interfacial normal and shear stresses in such a peel test to provide an improved understanding of its underlying mechanism. An approximate closed-form solution is also presented. The effect of the peel angle (i.e. the angle between the applied force and the substrate) on the interfacial stresses is discussed. Apart from being a widely used test for quantifying adhesive characteristics, the process of debonding in a peel test resembles that of intermediate flexural-shear or shear crack induced debonding in flexurally strengthened RC members, where a relative vertical displacement exists between the two sides of the crack, leading to an angle between the external plate and the concrete substrate. Therefore, the results of this study also offer some insight into the latter failure mode which is very important in the flexural strengthening design of RC members.


*Keywords:* FRP; Steel; Concrete; Bond; Peel test; Interfacial stress analysis; Strengthening

## 1. Introduction

Many structures need strengthening all over the world for various reasons such as ageing, change of function and design and construction errors (Teng et al., 2002a, 2003a). Steel plates have been used since 1960s but fibre reinforced polymer (FRP) plates have gradually replaced steel plates over the last decade and are now much more popular than steel plates because of their superior properties such as a high strength-to-density ratio and excellent corrosion resistance. FRP plates have been used to strengthen not only reinforced concrete (RC) but also metallic, masonry and timber structures. The success of the technique relies on the effective

* Corresponding author. Tel.: +44 131 650 6768; fax: +44 131 650 6781.
*E-mail address:* J.F.Chen@ed.ac.uk (J.F. Chen).

0020-7683/$ - see front matter 
doi:10.1016/j.ijsolstr.2006.12.028

stress transfer between the external plate and the surface layer of the existing structure (i.e. the substrate) through an adhesive layer. The bond behaviour between the plate and the substrate is thus of critical importance.

Although the steel- or FRP-to-concrete bond behaviour is commonly studied using either single- or double-shear pull tests (e.g. Roberts, 1989; Holzenkämpfer, 1994; Täljsten, 1996; Chajes et al., 1996; Brosens and van Gemert, 1997; Neubauer and Rostásy, 1997; Triantafillou, 1998; Kamiharaka et al., 1999; Ueda et al., 1999; Bizindavyi and Neale, 1999; Lee et al., 1999; Chen and Teng, 2001; Chen et al., 2001; Yuan et al., 2001; Wu et al., 2002; Yao et al., 2004; Yuan et al., 2004), the so-called 'peel test', which, in the present context, involves the inclined pulling of an FRP plate bonded to a concrete block or a substrate of another material to cause debonding (Fig. 1), has been used for a long time to characterise the bond behaviour of adhesives (Gent and Hamed, 1975; Nicholson, 1977; Thouless and Jensen, 1992; Karbhari and Engineer, 1996; Kimpara et al., 1998). The 'peel force' required to peel the plate/sheet from the substrate is measured in a peel test. Gent and Hamed (1975) discussed the relationship between the peel force and the peel angle (i.e. the angle between the applied force and the substrate) through small deformation bending analysis of the bonded elastic plate. Nicholson (1977) extended this analysis to include the large deformation effect. In both studies, the substrate was treated as rigid and the interfacial shear stress was neglected.

More recently, the relationship between the toughness of the interface and the peel force has been the subject of investigation using the energy approach (Thouless and Jensen, 1992; Karbhari and Engineer, 1996; Kimpara et al., 1998). Thouless and Jensen (1992) used a linear elastic analysis to determine the phase angle at the tip of an interface crack in the peel test. Karbhari and Engineer (1996) developed a peel test for investigating the bond behaviour between FRP and concrete and discussed different mechanisms of interfacial fracture. Kimpara et al. (1998) proposed a peel test method for FRP plates bonded to mortar and concrete to characterise the peeling strength and to examine the effects of different surface treatments and primers. The relationship between the deflection of the FRP plate, the debonded length (i.e. length of debonded zone) and the debonding load was obtained from geometrical and equilibrium considerations of a thin elastic membrane, from which the energy release rate due to peeling was found as a function of the deflection-to-debonded

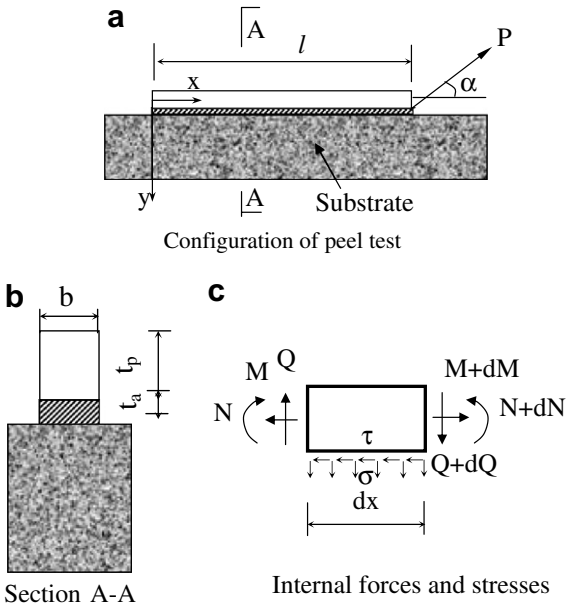


Fig. 1. Peel test: geometry and notation.

length ratio. However, in such an energy approach the interfacial peeling (normal) and shear stresses cannot be determined.

This paper presents an analytical solution for the interfacial normal and shear stresses between the plate and the substrate in such a peel test by treating the plate as an elastic beam resting on an elastic foundation representing the adhesive layer which possesses both normal and shear rigidities, with the substrate assumed to be rigid. A simpler closed-form solution is also presented. The former is referred to as the "exact" solution and the later the "approximate" solution in the paper for convenience. A parametric study is also presented to achieve a better understanding of the bond behaviour in a peel test.

It may be noted that interfacial debonding is one of the major failure modes for FRP strengthened RC structures (Teng et al., 2002a, 2003a,b; Yao et al., 2005). Debonding may start from various locations such as the end of an FRP plate, a flexural crack, a flexural-shear crack, or a shear crack in flexurally strengthened RC beams. Where debonding starts from a critical diagonal crack (CDC) (Mohamed Ali et al., 2001, 2002; Oehler et al., 2003) or flexural-shear crack, there exists a relative vertical displacement between the two sides of the crack, leading to an angle between the debonded part of the FRP plate and the concrete substrate. Another example where the debonded part of an FRP plate is pulled at an angle to the substrate occurs in the debonding failure process of a curved structural member strengthened with FRP, such as arches and tunnels strengthened with FRP on their intrados (e.g. Eshwar et al., 2005; De Lorenzis et al., 2006). A similarity exists between these situations, where the tensile force in the debonded part of the FRP plate is inclined from the substrate concrete surface, and a peel test (Fig. 1a). Therefore, the results of this study are also expected to provide some insight into the behaviour of intermediate flexural-shear crack or shear crack induced debonding in flexurally strengthened RC members.

## 2. The problem and assumptions

A thin plate bonded to a rigid substrate through an adhesive layer is shown in Fig. 1, where $t_p$, $b$ and $l$ are the thickness, width and length of the plate, respectively, while $t_a$ is the thickness of the adhesive layer. A load $P$ is applied at the right end of the plate at an angle $\alpha$ from the substrate (Fig. 1a). For convenience of presentation, the left end of the plate ($x = 0$) is termed the far end and the right end ($x = l$) the loaded end hereafter.

The following assumptions are adopted in the analysis presented in this study:

(a) the problem is in a plane stress state;
(b) the thicknesses of the adhesive layer and the plate are small compared to the bond length;
(c) the adhesive layer and the plate are both linearly elastic;
(d) the stresses in the adhesive layer are constant across its thickness; and
(e) the substrate is rigid.

Assumption (d) is commonly adopted in interfacial stress analysis (Smith and Teng, 2001) and the predictions compare well with finite element results (Teng et al., 2002b) for the mid-adhesive section. If this assumption is removed, then much more complicated solutions result, as has been done by Rabinvich and Frostig (2000), Shen et al. (2001), Yang et al. (2004, 2007). The use of this simplifying assumption allows a relatively simple solution to be obtained that still sheds considerable light on the interfacial behaviour.

The assumption of a rigid substrate [Assumption (e)] limits the solution to situations where the deformation of the substrate is insignificant compared to that of the adhesive layer and the thin plate. This implies that the substrate has an elastic modulus much larger than that of the adhesive so that the shear deformation of the substrate can be neglected, and a flexural stiffness much larger than that of the thin plate so that the bending deformation of the substrate can be neglected. This is generally the case for thin FRP or steel plates bonded to concrete and metallic members.

## 3. Governing equations

Equilibrium consideration of an infinitesimal plate element gives the following equations

$$\frac{\mathrm{d}N}{\mathrm{d}x} = b\tau \tag{1a}$$

$$\frac{\mathrm{d}Q}{\mathrm{d}x} = -b\sigma \tag{1b}$$

$$\frac{\mathrm{d}M}{\mathrm{d}x} = Q + \frac{bt_\mathrm{p}}{2}\tau \tag{1c}$$

where $N$, $Q$ and $M$ are the longitudinal membrane force, the transverse shear force and the bending moment in the plate, and $\sigma$ and $\tau$ are the normal and the shear stresses in the adhesive layer. The longitudinal strain at the bottom surface of the plate is given by

$$\varepsilon_x = \frac{\mathrm{d}u}{\mathrm{d}x} = \frac{1}{E_\mathrm{p}}\left(\frac{N}{bt_\mathrm{p}} + \frac{6M}{bt_\mathrm{p}^2}\right) \tag{2}$$

in which $E_\mathrm{p}$ is the elastic modulus of the plate in the $x$ direction and $u$ is the longitudinal displacement at the bottom surface of the plate. The relationship between the transverse deflection $w$ and the moment in the plate $M$ can be expressed as

$$\frac{\mathrm{d}^2w}{\mathrm{d}x^2} = -\frac{M}{E_\mathrm{p}I_\mathrm{p}} \tag{3}$$

where $I_\mathrm{p} = bt_\mathrm{p}^3/12$ is the second moment of area of the plate with respect to its own neutral axis.

Assuming that the normal strain $\varepsilon_y$ and the shear strain $\gamma_{xy}$ are constant across the thickness of the adhesive layer, the normal and shear stresses in the adhesive layer can be obtained from

$$\sigma = -E_\mathrm{a}\frac{w}{t_\mathrm{a}} \tag{4a}$$

$$\tau = G_\mathrm{a}\frac{u}{t_\mathrm{a}} \tag{4b}$$

where $E_\mathrm{a}$ and $G_\mathrm{a}$ are the elastic and shear moduli of the adhesive.

Differentiating Eq. (4a) four times and Eq. (4b) three times and then substituting Eqs. (1)–(3) into the resulting equations respectively, Eqs. (1)–(4) can be reduced to the following differential equations in terms of $\sigma$ and $\tau$ in the adhesive layer

$$\frac{\mathrm{d}^3\tau}{\mathrm{d}x^3} - a_1\frac{\mathrm{d}\tau}{\mathrm{d}x} + a_2\sigma = 0 \tag{5a}$$

$$\frac{\mathrm{d}^4\sigma}{\mathrm{d}x^4} + a_3\sigma - a_4\frac{\mathrm{d}\tau}{\mathrm{d}x} = 0 \tag{5b}$$

where

$$a_1 = \frac{4G_\mathrm{a}}{E_\mathrm{p}t_\mathrm{p}t_\mathrm{a}}, \quad a_2 = \frac{6G_\mathrm{a}}{E_\mathrm{p}t_\mathrm{p}^2t_\mathrm{a}}, \quad a_3 = \frac{12E_\mathrm{a}}{E_\mathrm{p}t_\mathrm{p}^3t_\mathrm{a}}, \quad a_4 = \frac{6E_\mathrm{a}}{E_\mathrm{p}t_\mathrm{p}^2t_\mathrm{a}} \tag{6}$$

Substituting Eq. (5a) into Eq. (5b) yields

$$\frac{\mathrm{d}^7\tau}{\mathrm{d}x^7} + b_5\frac{\mathrm{d}^5\tau}{\mathrm{d}x^5} + b_3\frac{\mathrm{d}^3\tau}{\mathrm{d}x^3} + b_1\frac{\mathrm{d}\tau}{\mathrm{d}x} = 0 \tag{7}$$

in which

$$b_5 = -a_1, \quad b_3 = a_3, \quad b_1 = a_2a_4 - a_1a_3 \tag{8}$$

## 4. Boundary conditions

The boundary conditions for the plate are

$$\text{At } x = 0: \quad N = 0, \quad Q = 0, \quad M = 0 \tag{9}$$

$$\text{At } x = l: \quad N = P\cos\alpha, \quad Q = -P\sin\alpha, \quad M = 0 \tag{10}$$

From Eqs. (1)–(4) and (6), the above boundary conditions can be reduced to

$$\frac{\mathrm{d}\tau}{\mathrm{d}x} = 0 \text{ at } x = 0 \tag{11a}$$

$$\frac{\mathrm{d}\tau}{\mathrm{d}x} = \frac{1}{4}\cdot\frac{P}{b}a_1\cos\alpha \text{ at } x = l \tag{11b}$$

$$\int_0^l \tau\,\mathrm{d}x = \frac{P}{b}\cos\alpha \tag{11c}$$

$$\frac{\mathrm{d}^2\sigma}{\mathrm{d}x^2} = 0 \text{ at } x = 0 \tag{11d}$$

$$\frac{\mathrm{d}^2\sigma}{\mathrm{d}x^2} = 0 \text{ at } x = l \tag{11e}$$

$$\frac{\mathrm{d}^3\sigma}{\mathrm{d}x^3} = a_4\tau \text{ at } x = 0 \tag{11f}$$

$$\frac{\mathrm{d}^3\sigma}{\mathrm{d}x^3} = -a_3\frac{P}{b}\sin\alpha + a_4\tau \text{ at } x = l \tag{11g}$$

## 5. Solution

The characteristic equation of Eq. (7) is

$$m^7 + b_5m^5 + b_3m^3 + b_1m = 0 \tag{12}$$

Eq. (12) can be solved in closed-form. The seven roots of this algebraic equation are

$$m = 0, \quad \pm(\beta \pm \gamma\mathrm{i}), \quad \pm\lambda \tag{13}$$

where $\beta$, $\gamma$ and $\lambda$ are real. The general solution of Eq. (7) can be expressed as

$$\tau = C_0 + C_1f_1(x) + C_2f_2(x) + C_3f_3(x) + C_4f_4(x) + C_5\sinh\lambda x + C_6\cosh\lambda x \tag{14}$$

in which $C_i$ $(i = 0,\ldots,6)$ are unknown constants and functions $f_i(x)$ $(i = 1,\ldots,4)$ are defined as

$$f_1(x) = \sinh(\beta x)\sin(\gamma x) \tag{15a}$$

$$f_2(x) = \sinh(\beta x)\cos(\gamma x) \tag{15b}$$

$$f_3(x) = \cosh(\beta x)\sin(\gamma x) \tag{15c}$$

$$f_4(x) = \cosh(\beta x)\cos(\gamma x) \tag{15d}$$

The integration and derivatives of $f_i(x)$ are shown in Appendix A. Substituting Eq. (14) into (5a) and using the expressions in Appendix A yield

$$\begin{aligned} a_2\sigma = {} & (-3\beta^2\gamma + \gamma^3 + a_1\gamma)[C_1f_2(x) - C_2f_1(x) + C_3f_4(x) - C_4f_3(x)] \\ & + (-\beta^3 + 3\beta\gamma^2 + a_1\beta)[C_1f_3(x) + C_2f_4(x) + C_3f_1(x) + C_4f_2(x)] \\ & + C_5(-\lambda^3 + a_1\lambda)\cosh\lambda x + C_6(-\lambda^3 + a_1\lambda)\sinh\lambda x \end{aligned} \tag{16}$$

The constants $C_i$ can be determined from the boundary conditions (Eqs. (11a)–(11g)). Substituting Eqs. (14) and (16) into Eqs. (11a)–(11g) results in

$$[\mathbf{A}]\{\mathbf{C}\} = \frac{P}{b}\{\mathbf{B}\} \tag{17}$$

where

$$[\mathbf{A}] = \begin{bmatrix} 0 & 0 & A_{13} & A_{14} & 0 & A_{16} & 0 \\ 0 & A_{22} & A_{23} & A_{24} & A_{25} & A_{26} & A_{27} \\ A_{31} & A_{32} & A_{33} & A_{34} & A_{35} & A_{36} & A_{37} \\ 0 & 0 & A_{43} & A_{44} & 0 & A_{46} & 0 \\ 0 & A_{52} & A_{53} & A_{54} & A_{55} & A_{56} & A_{57} \\ A_{61} & A_{62} & 0 & 0 & A_{65} & 0 & A_{67} \\ A_{71} & A_{72} & A_{73} & A_{74} & A_{75} & A_{76} & A_{77} \end{bmatrix}, \quad \{\mathbf{B}\} = \begin{Bmatrix} 0 \\ B_2 \\ B_3 \\ 0 \\ 0 \\ 0 \\ B_7 \end{Bmatrix}, \quad \{\mathbf{C}\} = \begin{Bmatrix} C_0 \\ C_1 \\ C_2 \\ C_3 \\ C_4 \\ C_5 \\ C_6 \end{Bmatrix} \tag{18}$$

The non-zero elements of matrix [**A**] and vector {**B**} are given in Appendix B.

The solution procedure for a given problem is first to find the roots of Eq. (12) so that the values of $\beta$, $\gamma$ and $\lambda$ are obtained. The linear simultaneous algebraic equations (Eq. (17)) are then solved to determine the coefficients $C_i$. The interfacial stresses in the adhesive layer $\tau$ and $\sigma$ can finally be obtained from Eqs. (14) and (16).

## 6. Approximate solution

In the above solution, explicit expressions for the interfacial stresses are not available. Results can only be obtained through the numerical solution of the set of simultaneous linear algebraic equations (Eq. (17)), which is rather tedious. Furthermore, the $7 \times 7$ matrix [**A**] approaches a singular state and numerical instability can easily occur when the bond length considered is large due to the presence of hyperbolic functions. A two-stage analysis procedure similar to that proposed by Roberts (1989) is employed here to derive an approximate solution.

### 6.1. Stage I

It is assumed in this stage that the elastic modulus of the adhesive $E_a$ is very large so that $w = 0$. Hence $M = 0$ from Eq. (3). The normal interfacial stress $\sigma$ can be determined from Eqs. (1b) and (1c) as:

$$\sigma = \frac{t_p}{2}\frac{d\tau}{dx} \tag{19}$$

Substituting Eq. (2) into Eq. (1a) using Eq. (4b) and $M = 0$ gives

$$\frac{d^2\tau}{dx^2} - \frac{a_1}{4}\tau = 0 \tag{20}$$

The general solution of Eq. (20) is

$$\tau^{(1)} = c_1 \sinh\left(\frac{\sqrt{a_1}x}{2}\right) + c_2 \cosh\left(\frac{\sqrt{a_1}x}{2}\right) \tag{21}$$

Constants $c_1$ and $c_2$ can be obtained using the boundary conditions (Eqs. (11a) and (11b))

$$c_1 = 0, \quad c_2 = \frac{P\sqrt{a_1}\cos\alpha}{2b\sinh\left(\frac{\sqrt{a_1}l}{2}\right)} \tag{22}$$

Substituting Eq. (22) into Eq. (21) gives

$$\tau^{(1)} = \frac{P\sqrt{a_1}\cos\alpha}{2b} \cdot \frac{\cosh\frac{\sqrt{a_1}x}{2}}{\sinh\frac{\sqrt{a_1}l}{2}} \tag{23}$$

The normal stress in the adhesive can now be determined by substituting Eq. (23) into Eq. (19):

$$\sigma^{(1)} = \frac{Pa_1 t_p \cos\alpha}{8b} \cdot \frac{\sinh\frac{\sqrt{a_1}x}{2}}{\sinh\frac{\sqrt{a_1}l}{2}} \tag{24}$$

### 6.2. Stage II

From Eq. (1c), the Stage I solution implies that the shear force acting at the loaded end ($x = l$) of the plate is

$$Q^{(1)}|_{x=l} = -\frac{1}{2} b t_p \tau|_{x=l} = -\frac{P t_p \sqrt{a_1}\cos\alpha}{4} \coth\left(\frac{\sqrt{a_1}l}{2}\right) \tag{25}$$

However, the actual shear force acting at the plate end is $-P\sin\alpha$. Therefore, there exists an unbalanced shear force at the loaded end at the end of Stage I:

$$Q^{(2)}|_{x=l} = -P\sin\alpha - Q^{(1)}|_{x=l} \tag{26}$$

The task of Stage II is to apply this unbalanced shear force to the plate so that equilibrium is satisfied.

An approximate solution for this problem can be obtained by treating the plate as a beam on an elastic foundation possessing stiffness only in the transverse (normal) direction. The following differential equation can be derived based on equilibrium consideration of a plate element

$$\frac{d^4\sigma}{dx^4} + a_3\sigma = 0 \tag{27}$$

Assuming that the plate length $l$ is sufficiently large and the normal stress $\sigma$ approaches zero at locations sufficiently far away from the loaded end, Eq. (27) has the solution of

$$\sigma^{(2)} = e^{\sqrt[4]{\frac{a_3}{4}}(x-l)}\left[c_3 \sin\left(\sqrt[4]{\frac{a_3}{4}}(x-l)\right) + c_4 \cos\left(\sqrt[4]{\frac{a_3}{4}}(x-l)\right)\right] \tag{28}$$

The boundary conditions are $M = 0$ at $x = l$ and $Q = Q^{(2)}|_{x=l}$. These conditions may be transformed into the following equations by substituting Eq. (4a) into Eq. (3) and substituting Eqs. (25) and (26) into Eq. (1c) neglecting the shear stress term:

$$\frac{d^2\sigma}{dx^2} = 0 \text{ at } x = l \tag{29a}$$

$$\frac{d^3\sigma}{dx^3} = \frac{Pt_p}{4b} a_3 \sqrt{a_1}\cos\alpha - \frac{P}{b} a_3 \sin\alpha \text{ at } x = l \tag{29b}$$

Substituting Eq. (28) into Eq. (29) gives the constants

$$c_3 = 0, \quad c_4 = \frac{P}{4b}\sqrt[4]{\frac{a_3}{4}}(8\sin\alpha - 2t_f\sqrt{a_1}\cos\alpha) \tag{30}$$

Substituting Eq. (30) into Eq. (28) gives the interfacial normal stress

$$\sigma^{(2)} = \frac{P}{4b}\sqrt[4]{\frac{a_3}{4}}(8\sin\alpha - 2t_f\sqrt{a_1}\cos\alpha) e^{\sqrt[4]{\frac{a_3}{4}}(x-l)} \cos\left(\sqrt[4]{\frac{a_3}{4}}(x-l)\right) \tag{31}$$

The influence of the second stage of the solution on the shear stress is generally small and can be neglected when the peel angle is 0° as in Roberts (1989). This is not necessary the case when the peel angle is large, so this influence is assessed in the last section of the paper.

The complete solution for the shear and normal stresses in the adhesive layer is obtained as follows by superimposing the results from the first and the second stages.

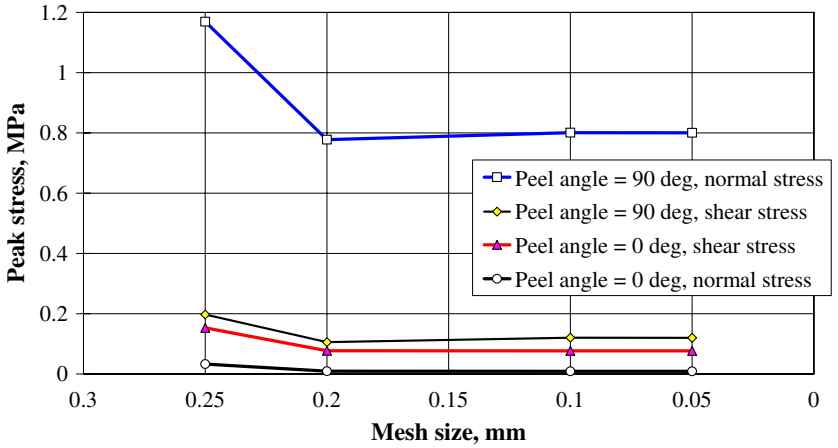


Fig. 2. Convergence of FEA meshes.

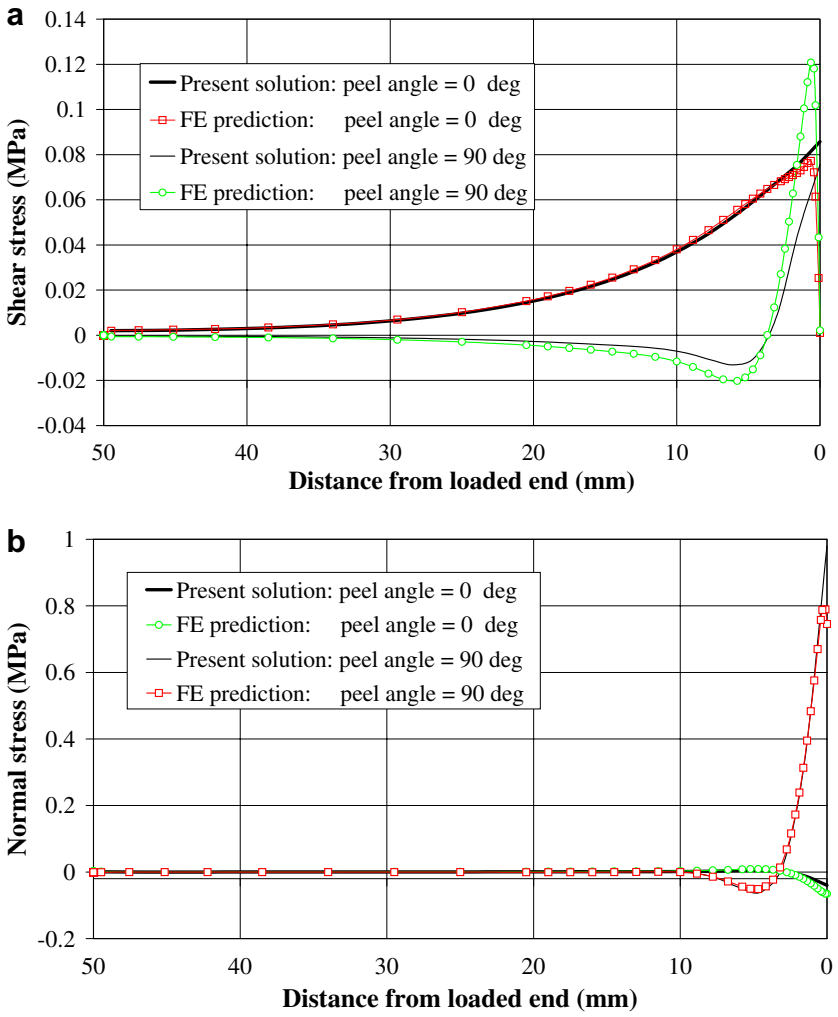


Fig. 3. Comparison between the present solution and FE predictions. (a) Interfacial shear stress. (b) Interfacial normal stress.

$$\tau = \frac{P\sqrt{a_1}\cos\alpha}{2b} \cdot \frac{\cosh\left(\frac{\sqrt{a_1}x}{2}\right)}{\sinh\left(\frac{\sqrt{a_1}l}{2}\right)} \tag{32a}$$

$$\sigma = \frac{Pa_1 t_p \cos\alpha}{8b} \cdot \frac{\sinh\left(\frac{\sqrt{a_1}x}{2}\right)}{\sinh\left(\frac{\sqrt{a_1}l}{2}\right)} + \frac{P}{4b}\sqrt[4]{\frac{a_3}{4}}(8\sin\alpha - 2t_p\sqrt{a_1}\cos\alpha)e^{\sqrt[4]{\frac{a_3}{4}}(x-l)}\cos\left(\sqrt[4]{\frac{a_3}{4}}(x-l)\right) \tag{32b}$$

The stresses in the adhesive layer at the loaded end are obtained by substituting $x = l$ into Eq. 32

$$\tau_{end} = \frac{P\sqrt{a_1}\cos\alpha}{2b}\coth\left(\frac{\sqrt{a_1}l}{2}\right) \approx \frac{P\cos\alpha}{2b}\sqrt{a_1} \tag{33a}$$

$$\sigma_{end} = \frac{Pa_1 t_p \cos\alpha}{8b} + \frac{P}{4b}\sqrt[4]{\frac{a_3}{4}}(8\sin\alpha - 2t_p\sqrt{a_1}\cos\alpha) \tag{33b}$$

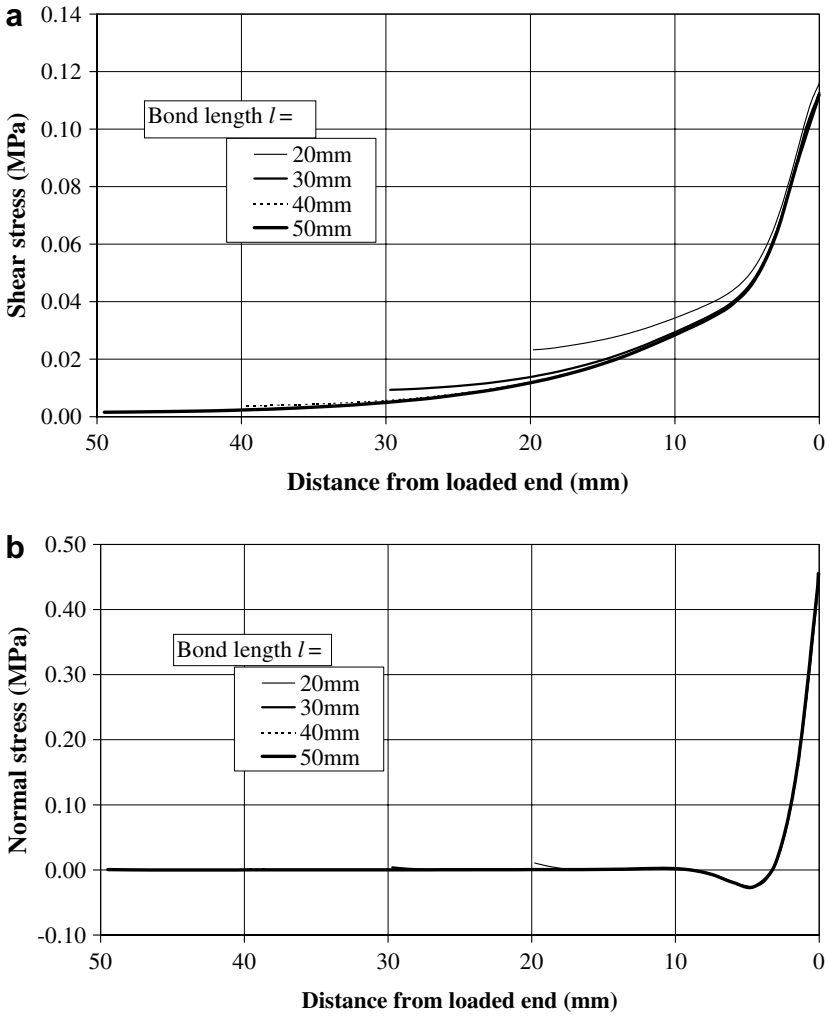


Fig. 4. Effect of bond length on interfacial stresses. (a) Shear stress. (b) Normal stress.

## 7. Comparison with finite element predictions

An example peel test specimen is considered. It consists of a 1-mm thick plate bonded to a rigid substrate through an adhesive layer. The elastic modulus of the plate is $E_p = 1.4 \times 10^5$ MPa while the bond length is 50 mm. This small bond length is used because significant interfacial stresses exist only in the vicinity of the loaded end and that numerical instability of the solution can occur due to the presence of hyperbolic functions in the solution if a larger bond length is used for such a thin plate. The latter is not a significant concern under the condition of the former. The adhesive layer has a thickness $t_a = 1$ mm, an elastic modulus $E_a = 3$ GPa and a shear modulus $G_a = 1.11$ GPa. The plate is subjected to a load $P$ with an intensity of 1 N/mm (i.e. the total load $P = 1.0 \times$ b).

The problem was modelled using an 8-node plane stress element in the finite element analysis program MSC.MARC. Meshes with square elements were adopted. The finite element results for the middle-thickness section are used in the comparison to reach a meaningful conclusion based on the observation made by Teng et al. (2002b). The fact that the problem can be analysed using a linear elastic finite element model does not mean that the present analytical model is not needed. An analytical solution has several advantages such as offering direct insight into the effects of different parameters rather than through numerous numerical analyses.

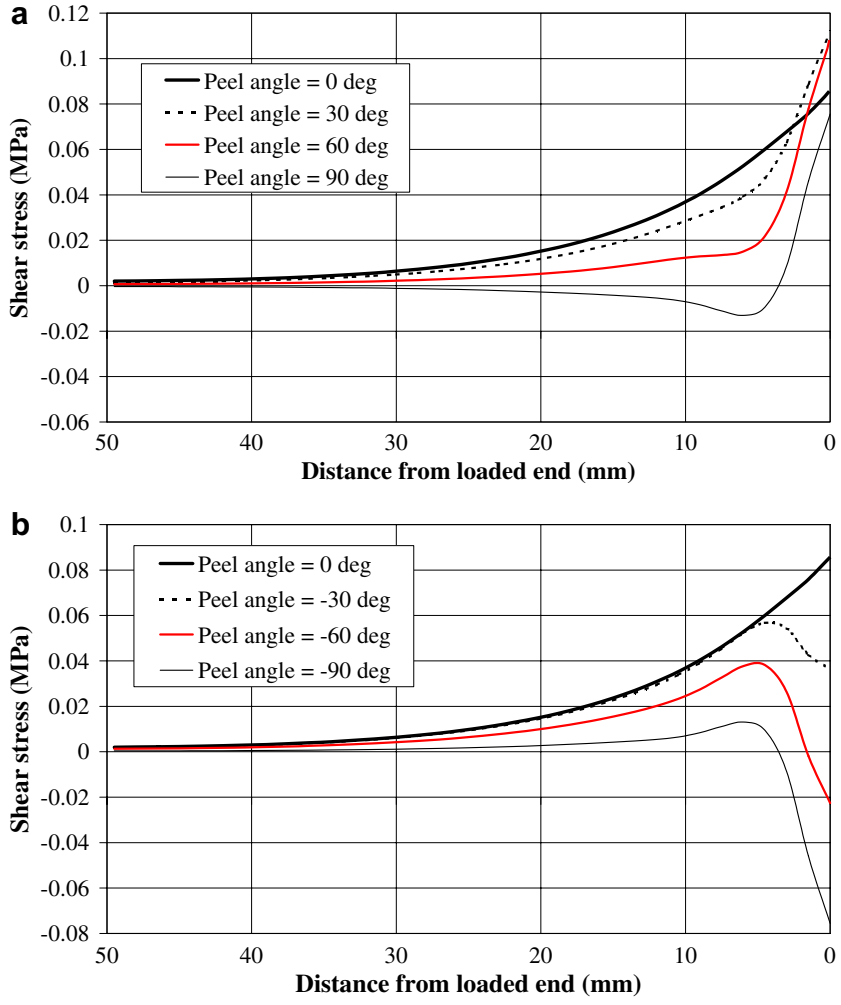


Fig. 5. Effect of peel angle on interfacial shear stress. (a) Peel angle $\alpha \geqslant 0$. (b) Peel angle $\alpha \leqslant 0$.

Analyses were conducted using four meshes with different element sizes of 0.25, 0.2, 0.1 and 0.05 mm, respectively. Fig. 2 shows the convergence of the peak stresses at the middle-thickness section of the adhesive close to the loaded end. It is clear that an element size of 0.2 mm is sufficiently small to yield converged results. The results from this mesh are used in the following comparison.

In Fig. 3, the exact solution is compared with the FE predictions for two cases: peel angle $\alpha = 0°$ and 90°. It may be noted that solutions for all other peel angles can be obtained from a linear combination of these two cases because the analysis is linear elastic. For the interfacial shear stress, the two analyses are in very close agreement when $\alpha = 0°$ (Fig. 3a). When $\alpha = 90°$, there are significant differences between the analytical solution and the finite element results. These differences are believed to be consequences of the following limitations of the analytical solution: (a) the stress-free boundary condition at the end of the adhesive layer is not satisfied by the analytical solution so it predicts the peak value at the free end, and (b) the stresses in the adhesive layer are assumed to be constant across its thickness.

Given that the results for all other angles are combinations of the two cases, the discrepancy experienced for $\alpha = 90°$ is expected to be the largest. The normal stresses from both solutions are in very close agreement for both peel angles (Fig. 3b).

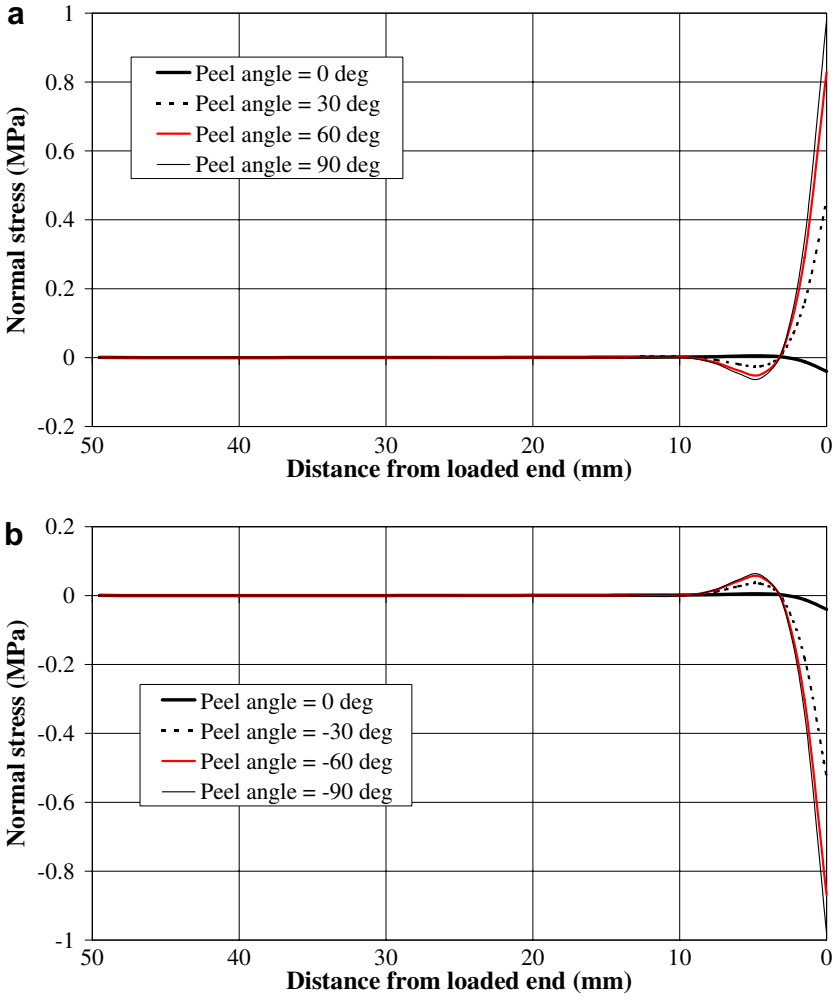


Fig. 6. Effect of peel angle on interfacial normal stress. (a) Peel angle $\alpha \geqslant 0$. (b) Peel angle $\alpha \leqslant 0$.

## 8. Parametric study

The effects of the bond length, the thickness and the elastic modulus of the plate, the thickness and the elastic modulus of the adhesive, and the peel angle on the interfacial stress distributions are investigated here using the example peel test specimen as the reference case. Unless otherwise stated, the plate is assumed to be subjected to a load of 1 N/mm with $\alpha = 30°$.

In the following discussion on trends and distributions of interfacial stresses, the words "decrease" and "increase" are used in mathematical terms. That is, when a stress goes from a large negative value to a small position value, this is described as an increase, although in terms of the absolute value (or magnitude) it is a decrease. When the absolute value or the magnitude is being discussed instead, it should be clear from the text that this is the case.

### *8.1. Effect of bond length on interfacial stresses*

Fig. 4 shows the effect of the plate bond length on interfacial stresses. Bond lengths of 20, 30, 40 and 50 mm are considered. Clearly, the stresses near the loaded end are the most important and are significant only within

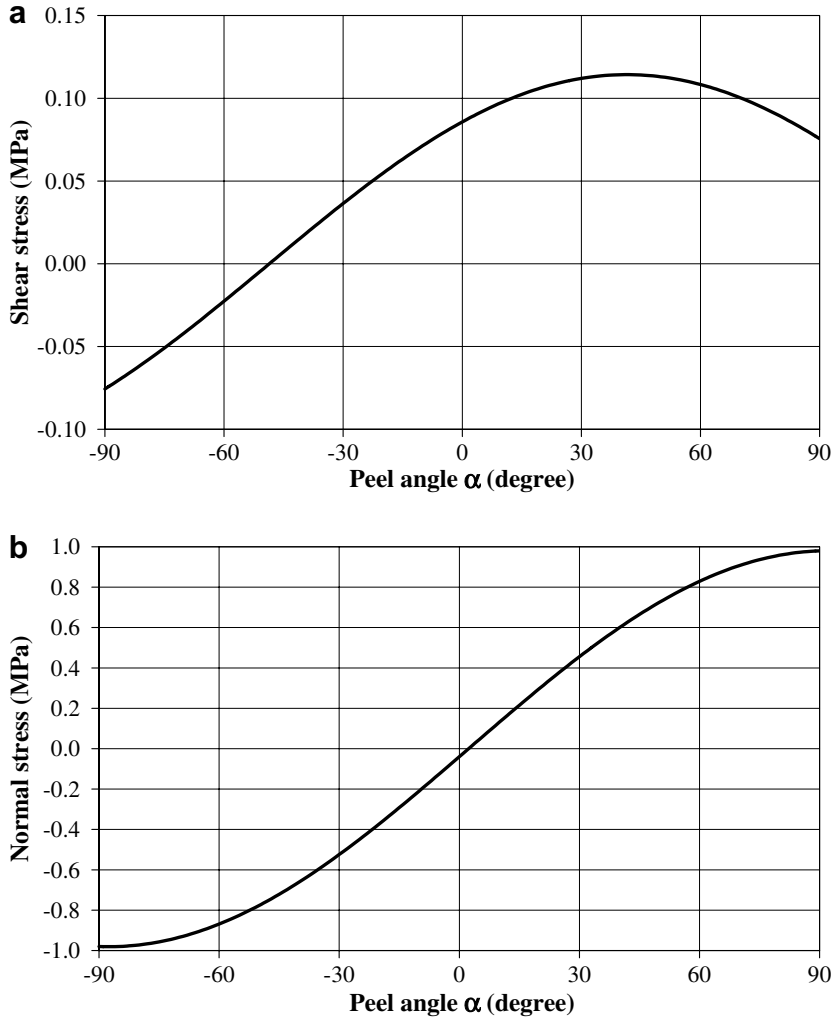


Fig. 7. Effect of peel angle on interfacial stresses at loaded end. (a) Shear stress. (b) Normal stress.

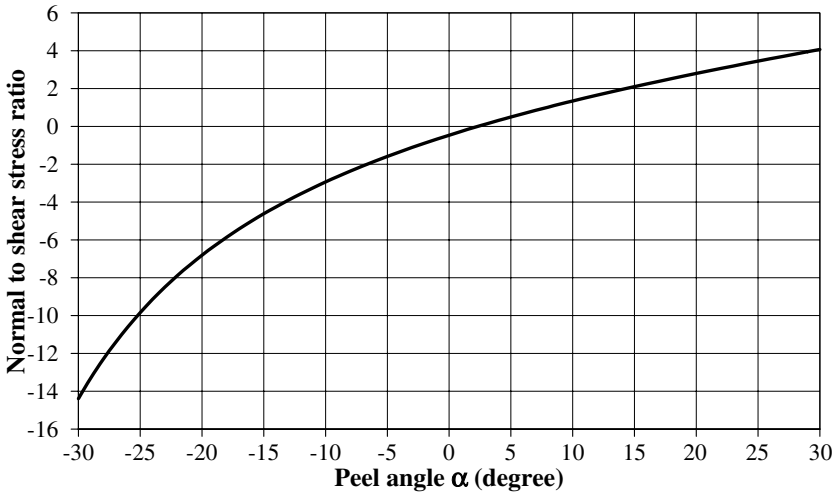


Fig. 8. Normal to shear interfacial stress ratio at loaded end.

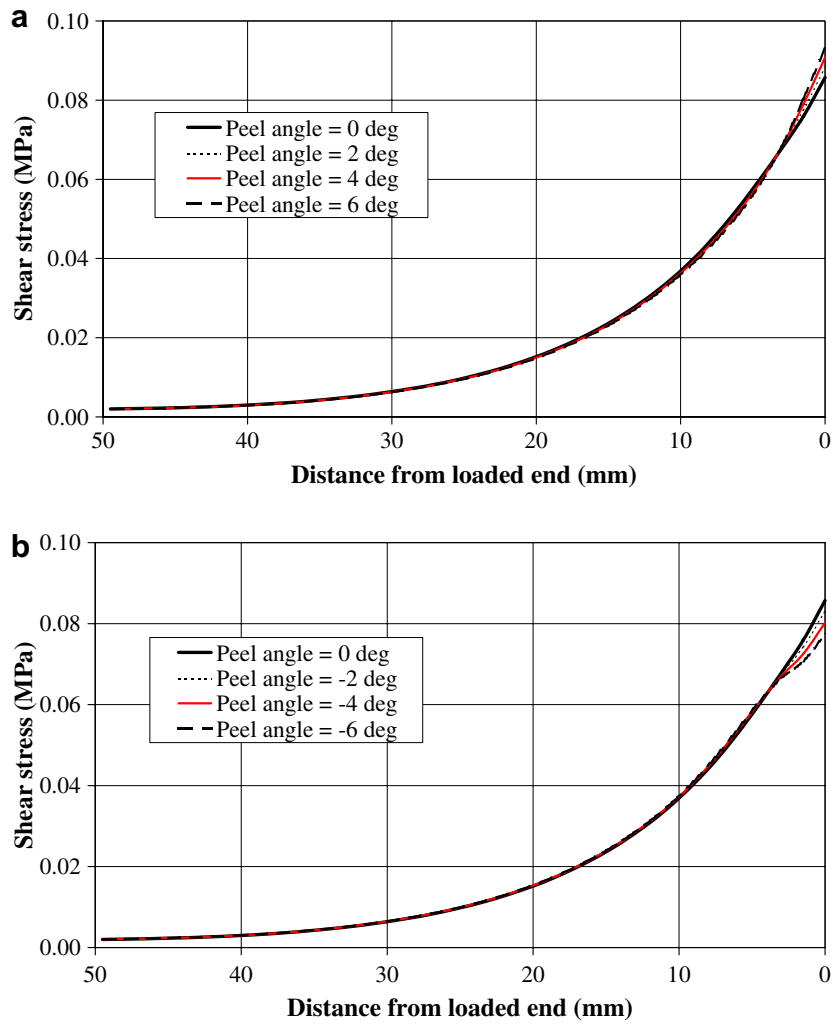


Fig. 9. Interfacial shear stresses for small peel angles. (a) Peel angle $\alpha \geqslant 0$. (b) Peel angle $\alpha \leqslant 0$.

a small zone. It can be seen that the interfacial normal stress decreases rapidly with the distance from the loaded end and is almost the same near the loaded end for different bond lengths. The interfacial shear stress near the loaded end changes little with the bond length when it varies from 20 to 50 mm, which is in agreement with the approximate solution (Eq. (33a)).

### 8.2. Effect of peel angle on interfacial stresses

Fig. 5 shows the interfacial shear stress distributions for several peel angles. When $\alpha = 0°$, the interfacial shear stress is largest at the loaded end and decreases smoothly towards the far end (Fig. 5a). When $\alpha$ increases to 30°, the shear stress is significantly higher at the loaded end than when $\alpha = 0°$ but it decreases much faster towards the far end. When $\alpha$ increases further to 60°, the shear stress is slightly smaller at the loaded end than that for $\alpha = 30°$ but it decreases even faster. When the load is vertical ($\alpha = 90°$), the shear stress is much smaller at the loaded end. It changes sign at around 4 mm and reaches a minimum at about 6 mm from the loaded end and then increases very slowly towards the far end. It should be noted that shear stresses are detrimental in either direction. The area between the shear stress distribution curve for $\alpha = 90°$ and the $x$-axis equals to zero, which is a necessary feature reflecting the horizontal equilibrium condition.

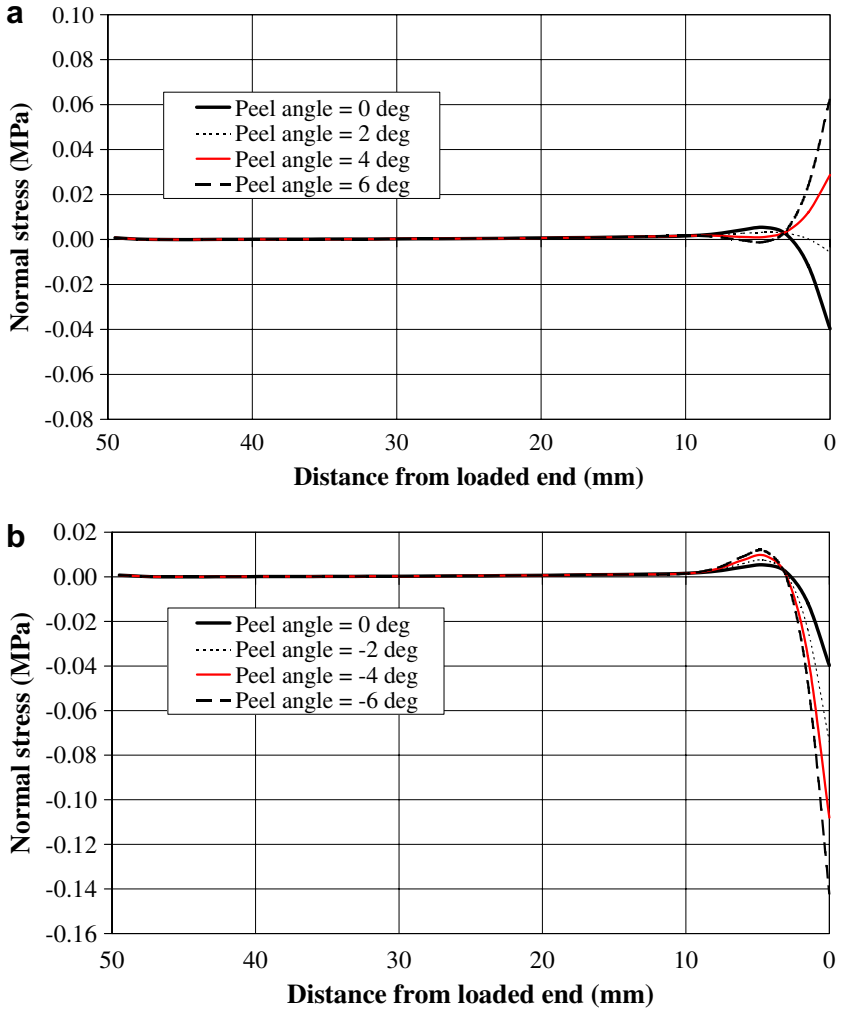


Fig. 10. Interfacial normal stresses for small peel angles. (a) Peel angle $\alpha \geqslant 0$. (b) Peel angle $\alpha \leqslant 0$.

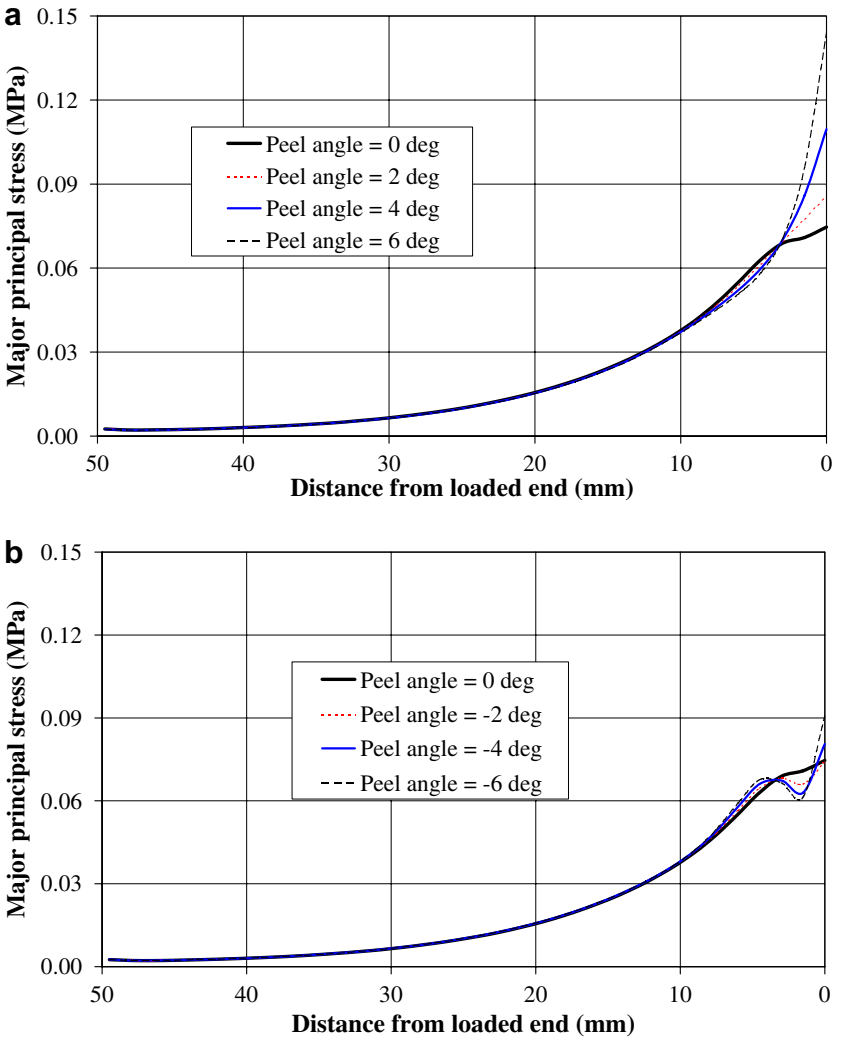


Fig. 11. Major principal stress in the adhesive layer for small peel angles. (a) Peel angle $\alpha \geqslant 0$. (b) Peel angle $\alpha \leqslant 0$.

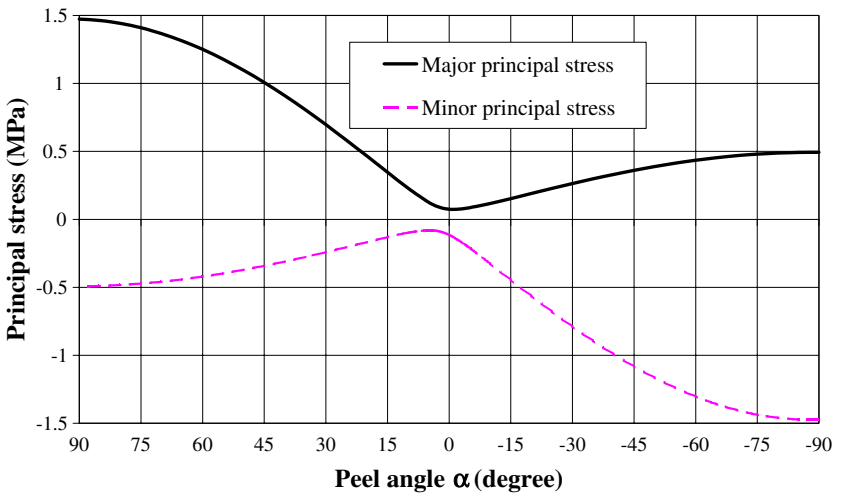


Fig. 12. Principal stresses in the adhesive layer at loaded end.

When the peel angle is negative (Fig. 5b), the interfacial shear stress at the loaded end decreases as $\alpha$ decreases and becomes negative when $\alpha = -60°$. For a given $\alpha < 0°$, the shear stress increases and reaches a peak value at about 5 mm from the loaded end and then decreases towards the far end.

It may be noted that a negative peel angle cannot be easily implemented in a practical peel test. However, negative angles do arise in the situation of an FRP plate bridging a flexural-shear or shear crack, where the relative vertical displacement between the two sides of the crack leads to a positive angle between the FRP plate and the concrete substrate on one side and a negative angle on the other side (Fig. 2). For completeness, the peel angle $\alpha$ is varied from $-90°$ to $90°$ in this study.

The corresponding interfacial normal stress is shown in Fig. 6. The normal stress is small when $\alpha = 0°$ (Fig. 6a). For all values of $\alpha > 0$, it decreases very fast from the loaded end and reaches its minimum at about 5 mm from the loaded end where the stress becomes compressive. This stress is almost zero at a distance of around 10 mm and beyond from the loaded end. The highest stress appears at the loaded end and it increases with $\alpha$.

For a negative peel angle, the interfacial normal stress distribution (Fig. 6b) is approximately the same as that for the corresponding positive peel angle except for a change in sign.

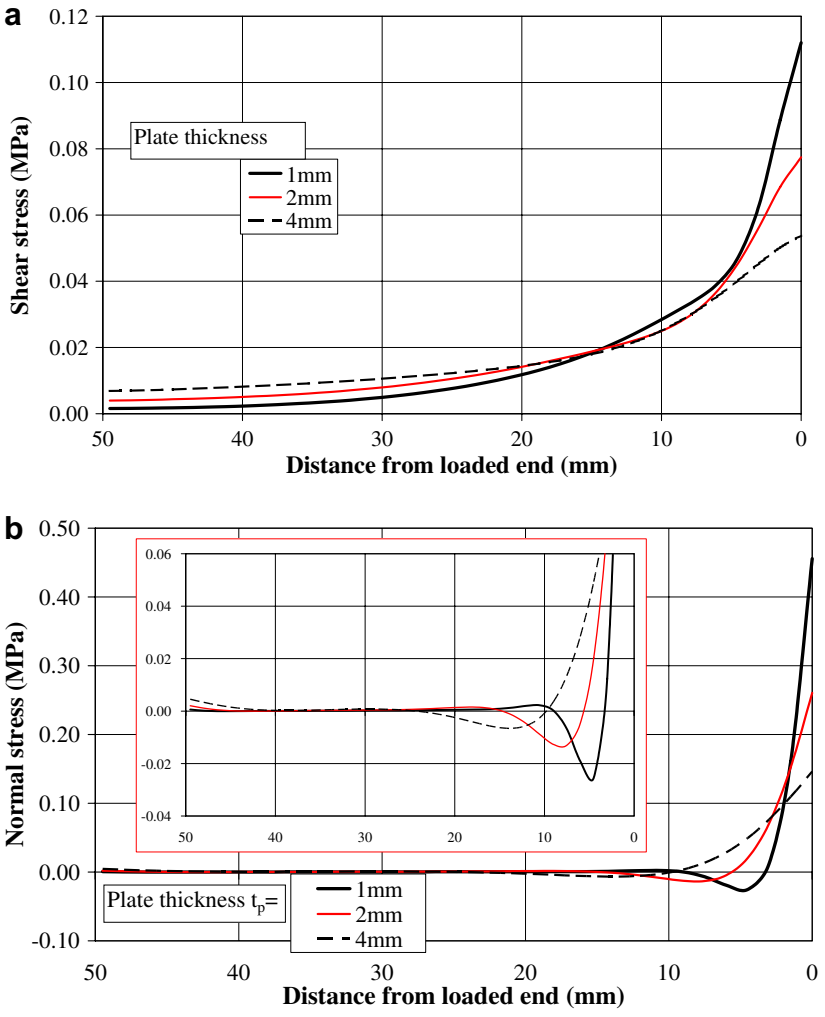


Fig. 13. Effect of FRP thickness on interfacial stresses ($\alpha = 30°$). (a) Shear stress. (b) Normal stress.

Fig. 7 shows the effect of the peel angle on the interfacial stresses at the loaded end. The shear stress increases from −0.076 MPa at $\alpha = -90°$ to a peak value of 0.114 MPa at $\alpha \approx 42°$ (Fig. 7a). Thereafter, it gradually decreases to about 0.076 MPa at $\alpha = 90°$. The interfacial normal stress at the loaded end has the lowest and highest values at about $\alpha = -88°$ and 92°, respectively (Fig. 7b). It is approximately anti-symmetrical about $\alpha \approx 2°$. This small shift of the axis of anti-symmetry from 0° to ~2° reflects the interaction between the interfacial shear and normal stresses.

The magnitude of the interfacial normal stress can be much larger than that of the interfacial shear stress if the peel angle is significant (Fig. 8). Even for a small peel angle, the magnitude of the interfacial normal stress can still be significant compared with that of the interfacial shear stress at the loaded end (Fig. 8). This could have significant implications for flexural-shear crack induced debonding failure where the relative vertical displacement between the sides of the crack leads to a small angle between the FRP plate and the concrete surface in FRP strengthened RC beams. A more detailed investigation is presented below.

### 8.3. Interfacial stresses for small peel angles

When the peel angle $\alpha$ varies from −6° to 6°, its effect on the interfacial shear stress distribution is very limited and localised at the loaded end (Fig. 9). However, its effect on the interfacial normal stress

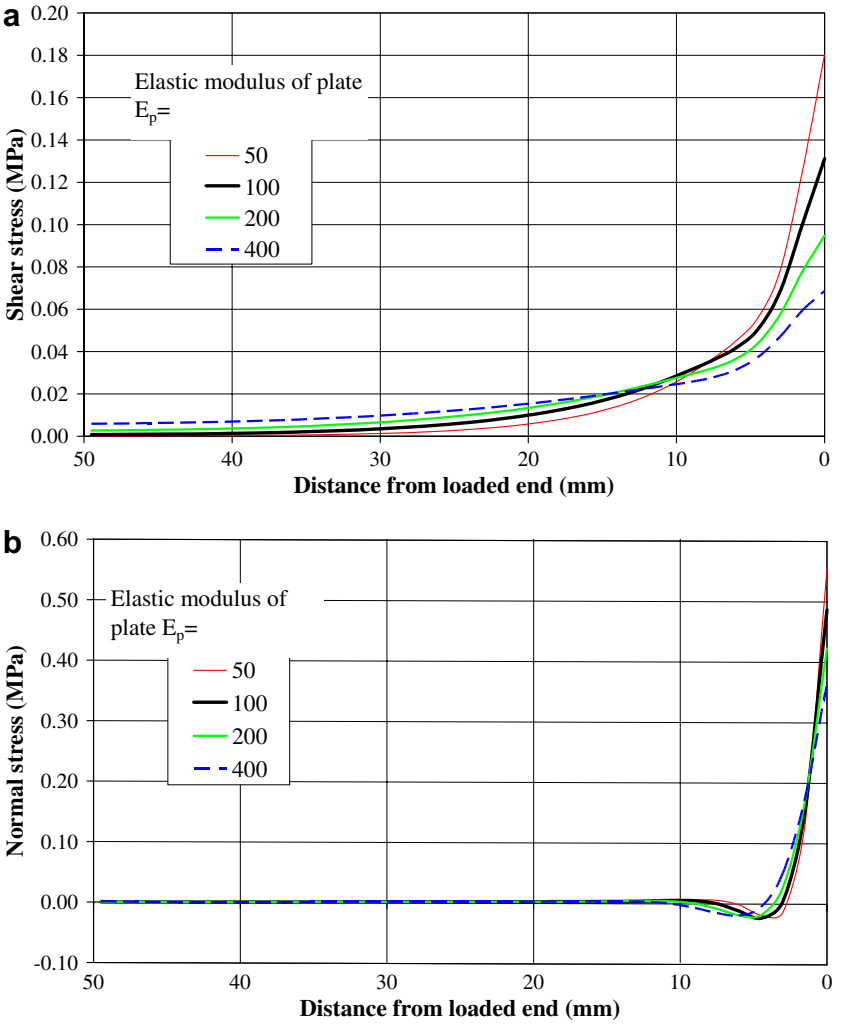


Fig. 14. Effect of elastic modulus of plate on interfacial stresses ($\alpha = 30°$). (a) Shear stress. (b) Normal stress.

distribution is very significant as shown in Fig. 10. It may be noted that the shear stress reduces slightly and the normal stress reduces very significantly at the loaded end when the peel angle is changed from zero to a small negative value. Both may be perceived as beneficial, but it would be indeed wrong to conclude that a small negative peel angle is beneficial because the interfacial shear and normal stresses do not reflect the complete stress state.

If the normal stress in the adhesive layer in the longitudinal direction is ignored as in the analysis, the principal stresses in the adhesive can be deduced from the interfacial shear and normal stresses. Such deduced major principal stress corresponding to Figs. 9 and 10 are shown in Fig. 11. It is seen that the major principal stress at the loaded end increases quickly when $\alpha$ increases from zero to a small positive value (Fig. 11a). When $\alpha$ changes from zero to a small negative value, the major principal stress also increases though not as significantly. Fig. 12 shows the effect of the peel angle on the major and minor principal stresses at the loaded end. It shows more clearly that both positive and negative peel angles have detrimental effects. Although the present linear elastic analysis does not directly reflect the failure load in such a test, this observation is in agreement with test results that both positive and negative small loading angles in a simple pull test reduces the bond strength (Yao et al., 2004).

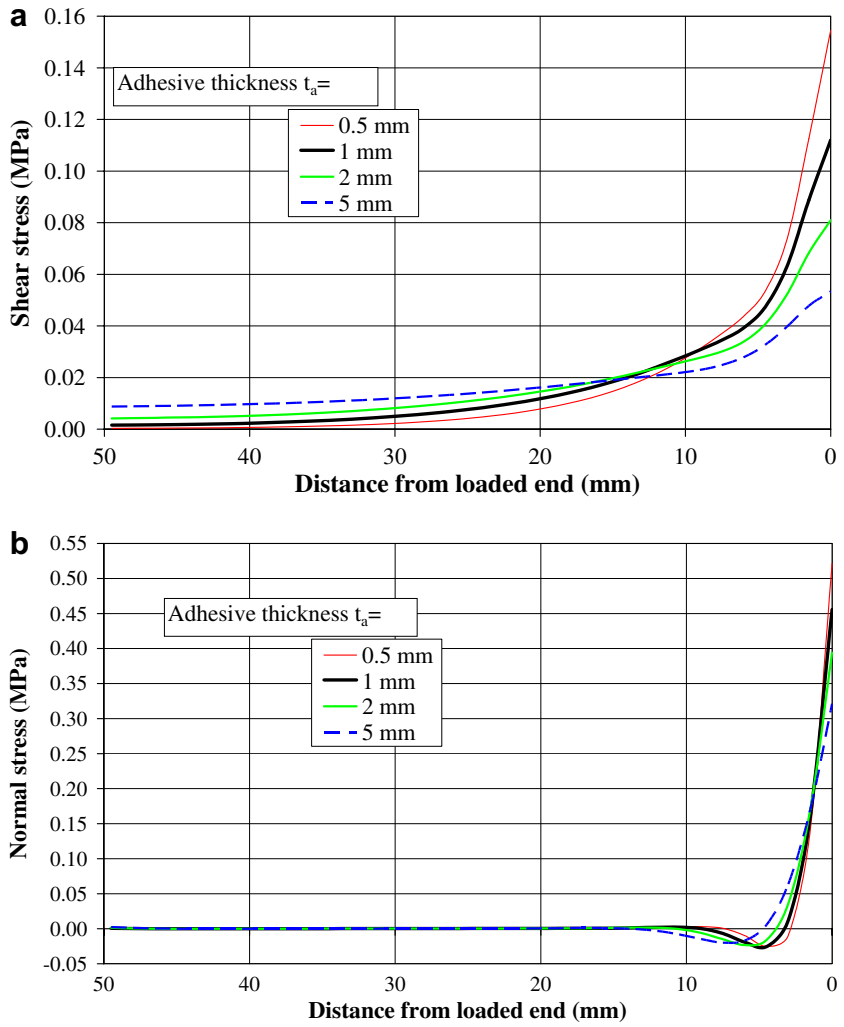


Fig. 15. Effect of adhesive thickness on interfacial stresses ($\alpha = 30°$). (a) Shear stress. (b) Normal stress.

### 8.4. Effect of plate thickness on interfacial stresses

Fig. 13 shows the effect of the plate thickness on the interfacial stresses. As the plate thickness increases, the interfacial shear stress decreases near the loaded end but increases near the far end (Fig. 13a). This means that a greater part of the applied force is transferred to the substrate away from the loaded end as the plate stiffness increases. Similarly, the peak value of the normal stress decreases but significant values are experienced over a wider portion of the bond length when the stiffness (thickness) of the plate increases (Fig. 13b). It may be noted that the reductions in the peak stresses are not inversely proportional to the plate thickness. If the plate is under a constant stress level, the peak interfacial stress values are higher for a thicker plate.

### 8.5. Effect of elastic modulus of plate on interfacial stresses

Fig. 14 shows the interfacial stresses when the elastic modulus of the plate varies from 50 GPa (a value for common GFRP) to 400 GPa (ultra high modulus CFRP). It is seen that the plate elastic modulus has a similar effect to the plate thickness: under the same applied load, a less stiff plate results in higher interfacial stresses at the loaded end because a greater part of the force is transferred to the substrate near the loaded end.

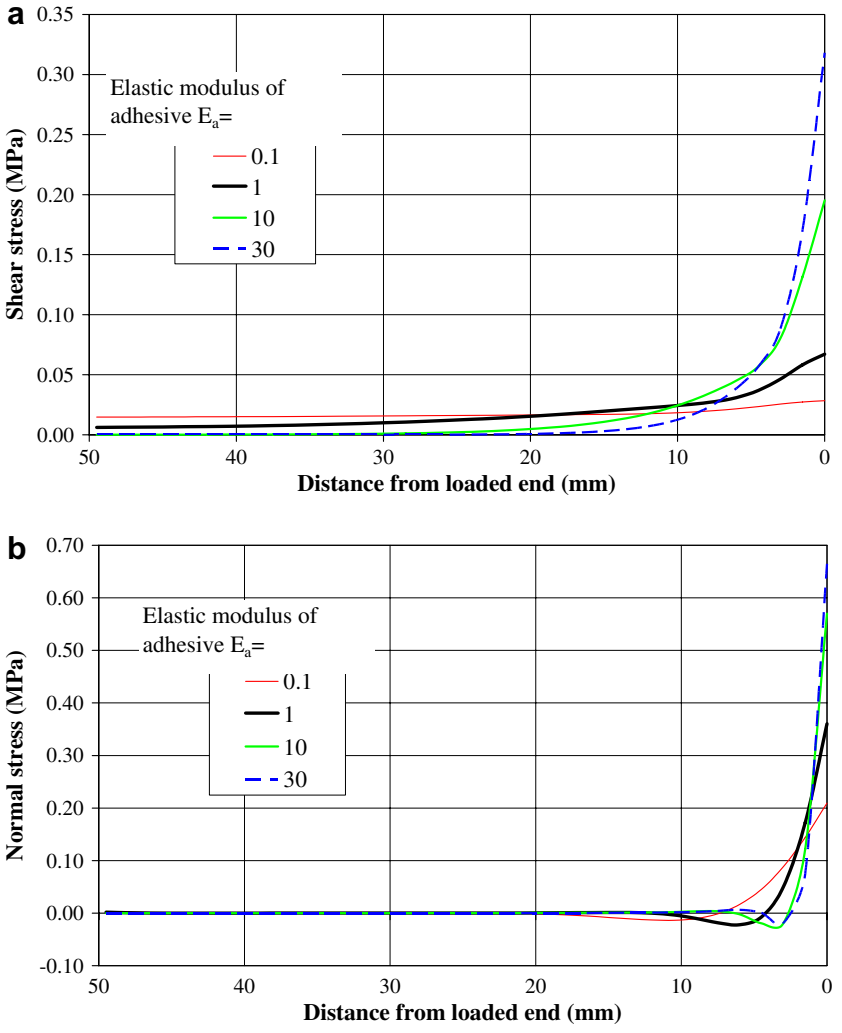


Fig. 16. Effect of elastic modulus of adhesive on interfacial stresses ($\alpha = 30°$). (a) Shear stress. (b) Normal stress.

### 8.6. Effect of adhesive thickness on interfacial stresses

Fig. 15 shows the effect of the adhesive thickness on the interfacial stresses. It is seen that the increase of the adhesive thickness has a similar effect as the increase of the plate thickness in that (a) the interfacial shear stress decreases near the loaded end but increases near the far end (Figs. 15a) and (b) the peak value of the normal stress decreases (Fig. 15b). This is because a larger zone near the loaded area is mobilised to transfer the force in the plate to the substrate when a thicker adhesive layer is used. One significant difference from the increase of plate thickness is that the reduction of the peak normal stress is much slower as the adhesive thickness increases.

### 8.7. Effect of elastic modulus of adhesive on interfacial stresses

Fig. 16 shows the effect of the elastic modulus of the adhesive $E_a$ within the range of 0.1–30 GPa. The shear modulus varies accordingly assuming a constant Poisson's ratio of 0.35. Clearly the effect of reducing the elastic modulus of the adhesive is similar to that of increasing the thickness of the adhesive layer. Both lead

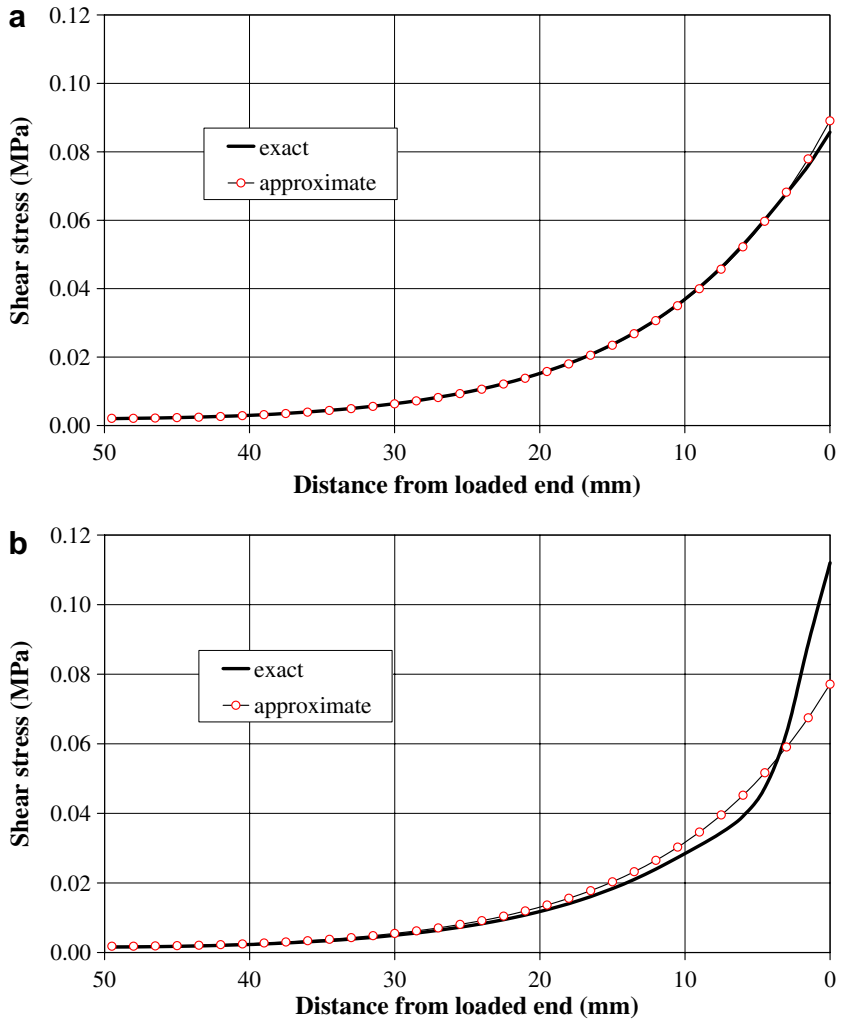


Fig. 17. Interfacial shear stresses predicted by exact and approximate solutions. (a) Peel angle $\alpha = 0°$. (b) Peel angle $\alpha = 30°$.

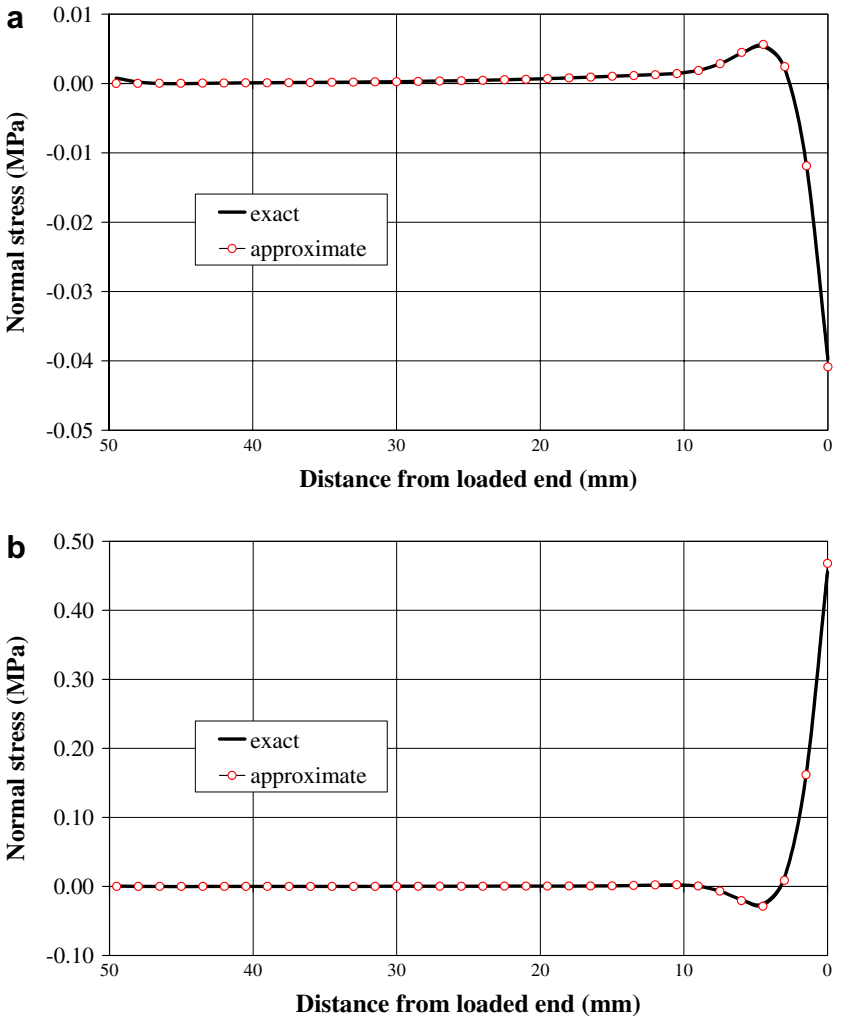


Fig. 18. Interfacial normal stresses predicted by exact and approximate solutions. (a) Peel angle $\alpha = 0°$. (b) Peel angle $\alpha = 30°$.

to smaller interfacial stresses near the loaded end, because a larger zone near the loaded end is mobilised to transfer the force in the plate to the substrate.

## 9. Accuracy of the approximate solution

Fig. 17 compares the interfacial shear stress distributions predicted by the exact solution and the approximate solution, respectively, for the two cases of $\alpha = 0°$ and 30°. The approximate solution yields shear stresses which are only slightly different from those from the exact solution for $\alpha = 0°$. When $\alpha = 30°$, the approximate solution predicts a peak shear stress at the loaded end about 30% lower than that from the exact solution. The two solutions yield interfacial normal stress distributions with no noticeable difference (Fig. 18). It may therefore be concluded that the approximate solution is a very good approximation to the exact solution.

## 10. Conclusions

This paper has presented an analytical solution for the interfacial stresses in a peel test in which a thin plate is bonded to a rigid substrate through an adhesive layer and loaded with a pulling force at an angle to the

substrate (the peel angle) at the loaded end. It has also presented an approximate solution which gives explicit expressions of the interfacial normal and shear stresses. The effects of the peel angle and other parameters on the interfacial stresses have been examined through a parametric study. The following conclusions may be drawn based on the numerical results and discussions:

(1) The interfacial normal and shear stresses are very localised in the vicinity of the loaded end;
(2) The magnitude of the interfacial normal stress can be very significant compared with that of the interfacial shear stress at the loaded end;
(3) The maximum interfacial normal stress always appears at the loaded end, but the maximum interfacial shear stress may appear at the loaded end or at a small distance from the loaded end depending on the value of the peel angle.
(4) The interfacial normal stress at the loaded end increases with the peel angle $\alpha$ within the practical range of $\alpha$ values but the interfacial shear stress at the loaded end peaks at $\alpha \approx 42^\circ$ for the example studied.
(5) Both positive and negative peel angles of small values are detrimental because the major principal interfacial stress is increased in both cases.
(6) Interfacial stresses decrease with an increase in the FRP plate stiffness (an increase of either the thickness or the elastic modulus) or with a decrease of the stiffness of the adhesive layer (a decrease of the elastic modulus or increase of the thickness) for the same applied load.
(7) The approximate solution provides a good estimation of the interfacial stresses.

## Acknowledgements

The authors are grateful for the financial support received from The Hong Kong Polytechnic University (Project code: BBZH), the Royal Society-NSFC China-UK Joint Project (Royal Society Grant No. IS 16657), the Science and Technology scheme of the Ministry of Construction (No. 05-K4-45), Guangdong Province (2005B32801002) and Guangzhou City (2005J1-C0251), China.

## Appendix A. Integration and derivative of function $f_i(x)$

The integration and derivative of function $f_i(x)$ are as follows:

$$(\beta^2+\gamma^2)\int f_1(x)\,\mathrm{d}x = \beta f_3(x) - \gamma f_2(x) \tag{A1a}$$

$$(\beta^2+\gamma^2)\int f_2(x)\,\mathrm{d}x = \beta f_4(x) + \gamma f_1(x) \tag{A1b}$$

$$(\beta^2+\gamma^2)\int f_3(x)\,\mathrm{d}x = \beta f_1(x) - \gamma f_4(x) \tag{A1c}$$

$$(\beta^2+\gamma^2)\int f_4(x)\,\mathrm{d}x = \beta f_2(x) + \gamma f_3(x) \tag{A1d}$$

$$f_1'(x) = \gamma f_2(x) + \beta f_3(x) \tag{A2a}$$
$$f_2'(x) = -\gamma f_1(x) + \beta f_4(x) \tag{A2b}$$
$$f_3'(x) = \gamma f_4(x) + \beta f_1(x) \tag{A2c}$$
$$f_4'(x) = -\gamma f_3(x) + \beta f_2(x) \tag{A2d}$$

$$f_1''(x) = (\beta^2-\gamma^2) f_1(x) + 2\beta\gamma f_4(x) \tag{A3a}$$
$$f_2''(x) = (\beta^2-\gamma^2) f_2(x) - 2\beta\gamma f_3(x) \tag{A3b}$$
$$f_3''(x) = (\beta^2-\gamma^2) f_3(x) + 2\beta\gamma f_2(x) \tag{A3c}$$
$$f_4''(x) = (\beta^2-\gamma^2) f_4(x) - 2\beta\gamma f_1(x) \tag{A3d}$$

$$f_1'''(x) = (3\beta^2\gamma - \gamma^3)f_2(x) + (\beta^3 - 3\beta\gamma^2)f_3(x) \tag{A4a}$$
$$f_2'''(x) = -(3\beta^2\gamma - \gamma^3)f_1(x) + (\beta^3 - 3\beta\gamma^2)f_4(x) \tag{A4b}$$
$$f_3'''(x) = (3\beta^2\gamma - \gamma^3)f_4(x) + (\beta^3 - 3\beta\gamma^2)f_1(x) \tag{A4c}$$
$$f_4'''(x) = -(3\beta^2\gamma - \gamma^3)f_3(x) + (\beta^3 - 3\beta\gamma^2)f_2(x) \tag{A4d}$$

## Appendix B. Matrixes [A] and {B}

The non-zero elements of matrix [**A**] are:

$$A_{13} = \beta \tag{B1a}$$
$$A_{14} = \gamma \tag{B1b}$$
$$A_{16} = \lambda \tag{B1c}$$

$$A_{22} = \gamma f_2(l) + \beta f_3(l) \tag{B2a}$$
$$A_{23} = -\gamma f_1(l) + \beta f_4(l) \tag{B2b}$$
$$A_{24} = \gamma f_4(l) + \beta f_1(l) \tag{B2c}$$
$$A_{25} = -\gamma f_3(l) + \beta f_2(l) \tag{B2d}$$
$$A_{26} = \lambda \cosh \lambda l \tag{B2e}$$
$$A_{27} = \lambda \sinh \lambda l \tag{B2f}$$

$$A_{31} = l(\beta^2 + \gamma^2) \tag{B3a}$$
$$A_{32} = \beta f_3(l) - \gamma f_2(l) \tag{B3b}$$
$$A_{33} = \beta f_4(l) + \gamma f_1(l) - \beta \tag{B3c}$$
$$A_{34} = \beta f_1(l) - \gamma f_4(l) + \gamma \tag{B3d}$$
$$A_{35} = \beta f_2(l) + \gamma f_3(l) \tag{B3e}$$
$$A_{36} = -\lambda^{-1}(\beta^2 + \gamma^2)(1 - \cosh \lambda l) \tag{B3f}$$
$$A_{37} = \lambda^{-1}(\beta^2 + \gamma^2) \sinh \lambda l \tag{B3g}$$

$$A_{43} = g_1(\beta, \gamma) \tag{B4a}$$
$$A_{44} = g_2(\beta, \gamma) \tag{B4b}$$
$$A_{46} = \lambda^3(-\lambda^2 + a_1) \tag{B4c}$$

$$A_{52} = g_2(\beta, \gamma) f_2(l) + g_1(\beta, \gamma) f_3(l) \tag{B5a}$$
$$A_{53} = -g_2(\beta, \gamma) f_1(l) + g_1(\beta, \gamma) f_4(l) \tag{B5b}$$
$$A_{54} = g_2(\beta, \gamma) f_4(l) + g_1(\beta, \gamma) f_1(l) \tag{B5c}$$
$$A_{55} = -g_2(\beta, \gamma) f_3(l) + g_1(\beta, \gamma) f_2(l) \tag{B5d}$$
$$A_{56} = \lambda^3(-\lambda^2 + a_1) \cosh \lambda l \tag{B5e}$$
$$A_{57} = \lambda^3(-\lambda^2 + a_1) \sinh \lambda l \tag{B5f}$$

$$A_{61} = -a_2 a_4 \tag{B6a}$$
$$A_{62} = g_3(\beta, \gamma) \tag{B6b}$$
$$A_{65} = g_4(\beta, \gamma) - a_2 a_4 \tag{B6c}$$
$$A_{67} = \lambda^4(-\lambda^2 + a_1) - a_2 a_4 \tag{B6d}$$

$$A_{71} = -a_2 a_4 \tag{B7a}$$
$$A_{72} = [g_4(\beta,\gamma) - a_2 a_4] f_1(l) + g_3(\beta,\gamma) f_4(l) \tag{B7b}$$
$$A_{73} = [g_4(\beta,\gamma) - a_2 a_4] f_2(l) - g_3(\beta,\gamma) f_3(l) \tag{B7c}$$
$$A_{74} = [g_4(\beta,\gamma) - a_2 a_4] f_3(l) + g_3(\beta,\gamma) f_2(l) \tag{B7d}$$
$$A_{75} = [g_4(\beta,\gamma) - a_2 a_4] f_4(l) - g_3(\beta,\gamma) f_1(l) \tag{B7e}$$
$$A_{76} = [\lambda^4(-\lambda^2 + a_1) - a_2 a_4] \sinh \lambda l \tag{B7f}$$
$$A_{77} = [\lambda^4(-\lambda^2 + a_1) - a_2 a_4] \cosh \lambda l \tag{B7g}$$

where

$$g_1(\beta,\gamma) = 2\beta\gamma^2(3\beta^2 - \gamma^2 - a_1) + \beta(-\beta^2 + 3\gamma^2 + a_1)(\beta^2 - \gamma^2) \tag{B8a}$$
$$g_2(\beta,\gamma) = 2\beta^2\gamma(-\beta^2 + 3\gamma^2 + a_1) + \gamma(-3\beta^2 + \gamma^2 + a_1)(\beta^2 - \gamma^2) \tag{B8b}$$
$$g_3(\beta,\gamma) = \beta\gamma(-3\beta^2 + \gamma^2 + a_1)(\beta^2 - 3\gamma^2) + \beta\gamma(-\beta^2 + 3\gamma^2 + a_1)(3\beta^2 - \gamma^2) \tag{B8c}$$
$$g_4(\beta,\gamma) = \beta^2(-\beta^2 + 3\gamma^2 + a_1)(\beta^2 - 3\gamma^2) - \gamma^2(-3\beta^2 + \gamma^2 + a_1)(3\beta^2 - \gamma^2) \tag{B8d}$$

The non-zero elements of $\{\mathbf{B}\}$ are:

$$B_2 = \frac{1}{4} a_1 \cos\alpha \tag{B9a}$$
$$B_3 = (\beta^2 + \gamma^2) \cos\alpha \tag{B9b}$$
$$B_7 = -a_2 a_3 \sin\alpha \tag{B9c}$$

## References


Bizindavyi, L., Neale, K.W., 1999. Transfer lengths and bond strengths for composites bonded to concrete. Journal of Composites for Construction, ASCE 3 (4), 153–160.

Brosens, K., van Gemert, D., 1997. Anchoring stresses between concrete and carbon fibre reinforced laminates, Proceedings of the 3rd International Symposium on Non-Metallic (FRP) Reinforced Concrete Structures, Oct. Japan, 1, 271–278.

Chajes, M.J., Finch, W.W., Januszka, T.F., Thomson, T.A., 1996. Bond and force transfer of composite material plates bonded to concrete. ACI Structural Journal 93 (2), 208–217.

Chen, J.F., Teng, J.G., 2001. Anchorage strength models for FRP and steel plates bonded to concrete. Journal of Structural Engineering, ASCE 127 (7), 784–791.

Chen, J.F., Yang, Z.J., Holt, G.D., 2001. FRP or steel plate-to-concrete bonded joints: effect of test methods on experimental bond strength. Steel & Composite Structures – an International Journal 1 (2), 231–244.

De Lorenzis, L., Teng, J.G., Zhang, L., 2006. Interfacial stresses in curved members bonded with a thin plate. International Journal of Solids and Structures 43 (25–26), 7501–7517.

Eshwar, N., Ibell, T.J., Nanni, A., 2005. Effectiveness of CFRP strengthening on curved soffit RC beams. Advances in Structural Engineering 8 (1), 55–68.

Gent, A.N., Hamed, G.R., 1975. Peel mechanics. Journal of Adhesion 7, 91–95.

Holzenkämpfer, O. 1994. Ingenieurmodelle des Verbundes geklebter Bewehrung für Betonbauteile, Germany: Dissertation, TU Braunschweig.

Kamiharaka, A., Shimomura, T., Marurama, K., Nishida, H., 1999. Stress transfer and peeling-off behavior of continuous fiber reinforced sheet-concrete system. Symposium of EASEC-7, Kochi, Japan, pp. 1283–1288.

Karbhari, V.M., Engineer, M., 1996. Investigation of bond between concrete and composites: use of a peel test. Journal of Reinforced Plastics and Composites 15 (2), 208–227.

Kimpara, I., Kageyama, K., Suzuki, T., Ohsawa, I., Yamaguchi, K., 1998. Characterization of peeling strength of FRP sheets bonded on mortar and concrete. In: Proceedings of the Eighth Japan-US Conference on Composite Materials, 24–25 September, Baltimore, Maryland, USA, pp. 1010–1019.

Lee, Y.J., Boothby, T.E., Bakis, C.E., Nanni, A., 1999. Slip modulus of FRP Sheets bonded to concrete. Journal of Composites for Construction, ASCE 3 (4), 161–167.

Mohamed Ali, M.S., Oehlers, D.J., Bradford, M.A., 2001. Shear peeling of steel plates bonded to the tension faces of RC beams. ASCE Journal of Structural Engineering 127 (12), 1453–1460.

Mohamed Ali, M.S., Oehlers, D.J., Bradford, M.A., 2002. Interaction between flexure and shear on the debonding of RC beams retrofitted with compression face plates. Advances in Structural Engineering 5 (4), 223–230.

Neubauer, U., Rostásy, F.S., 1997. Design aspects of concrete structures strengthened with externally bonded CFRP plates. In: Proceedings of the 7th International Conference on Structural Faults and Repairs, ECS Publications, Edinburgh, vol. 2, pp. 109–118.

Nicholson, D.W., 1977. Peel mechanics with large bending. International Journal of Fracture 13 (3), 279–287.

Oehler, D.J., Park, S.M., Mohamed Ali, M.S., 2003. A structural engineering approach to adhesive bonding longitudinal plates to RC beams and slabs. Composites: Part A 34 (12), 887–897.

Rabinvich, O., Frostig, Y., 2000. Closed-form high-order analysis of RC beams strengthened with FRP strips. Journal of Composites for Construction, ASCE 4, 65–74.

Roberts, T.M., 1989. Shear and normal stresses in adhesive joints. Journal of Engineering Mechanics, ASCE 115 (11), 2460–2479.

Shen, H.S., Teng, J.G., Yang, J., 2001. Interfacial stresses in beams and slabs bonded with thin plate. Journal of Engineering Mechanics, ASCE 127, 399–406.

Smith, S.T., Teng, J.G., 2001. Interfacial stresses in plated beams. Engineering Structures 23 (7), 857–871.

Täljsten, B., 1996. Strengthening of concrete prisms using the plate-bonding technique. International Journal of Fracture 82, 253–266.

Teng, J.G., Chen, J.F., Smith, S.T., Lam, L., 2002a. FRP Strengthened RC Structures. Wiley, Chichester, UK.

Teng, J.G., Zhang, J.W., Smith, S.T., 2002b. Interfacial stresses in RC beams bonded with a soffit plate: a finite element study. Construction and Building Materials 16 (1), 1–14.

Teng, J.G., Chen, J.F., Smith, S.T., Lam, L., 2003a. Behaviour and strength of FRP-strengthened RC structures: a state-of-the-art review. Proceedings of the Institution of Civil Engineers – Structures and Buildings, 156(SB1), 51–62.

Teng, J.G., Smith, S.T., Yao, J., Chen, J.F., 2003b. Intermediate crack-induced debonding in RC Beams and slabs. Construction and Building Materials 17 (6–7), 447–462.

Thouless, M.D., Jensen, M.D., 1992. Elastic fracture mechanics of the peel-test geometry. Journal of Adhesion 39, 185–197.

Triantafillou, T.C., 1998. Fracture mechanics approaches to concrete strengthening using FRP materials. In: Proceedings FRAMCOS-3, AEDIFICATIO Publishers, D-79104 Freiburg, Germany, pp. 1761–1770.

Ueda, T., Sato, Y., Asano, Y., 1999. Experimental study on bond strength of continuous carbon fiber sheet. In: 4th International Symposium on Fiber Reinforced Polymer for Reinforced Concrete Structures, SP-188, ACI International, Baltimore, pp. 407–416.

Wu, Z.S., Yuan, H., Niu, H., 2002. Stress transfer and fracture propagation in different kinds of adhesive joints. Journal of Engineering Mechanics, ASCE 128 (5), 562–573.

Yao, J., Teng, J.G., Chen, J.F., 2004. Experimental study on FRP-to-concrete bonded joints. Composites Part B: Engineering 36 (2), 99–113.

Yao, J., Teng, J.G., Lam, L., 2005. Experimental study on intermediate crack debonding in FRP-strengthened RC flexural members. Advances in Structural Engineering 8 (4), 365–396.

Yuan, H., Wu, Z.S., Yoshizawa, H., 2001. Theoretical solutions on interfacial stress transfer of externally bonded steel/composite laminates. Journal of Structural Mechanics and Earthquake Engineering, JSCE 18 (1), 27–39.

Yuan, H., Teng, J.G., Seracino, R., Wu, Z.S., Yao, J., 2004. Full-range behavior of FRP-to-concrete bonded joints. Engineering Structures 26 (5), 553–565.

Yang, J., Teng, J.G., Chen, J.F., 2004. A high order closed-form solution for interfacial stresses in soffit plated RC beams under arbitrary loads. Proceedings of the Institution of Civil Engineers – Structures and Buildings 157(SB1) 77–89.

Yang, J., Chen, J.F., Teng, J.G., 2007. Interfacial stress analysis of plated beams under symmetric mechanical and thermal loading, in preparation.